J. Am. Soc. Mass Spectrom. (2018) 29:2086–2095
DOI: 10.1007/s13361-018-2007-x

RESEARCH ARTICLE

Optimized Electrostatic Linear Ion Trap for Charge Detection Mass Spectrometry

Joanna A. Hogan, Martin F. Jarrold

Chemistry Department, Indiana University, Bloomington, IN 47405, USA

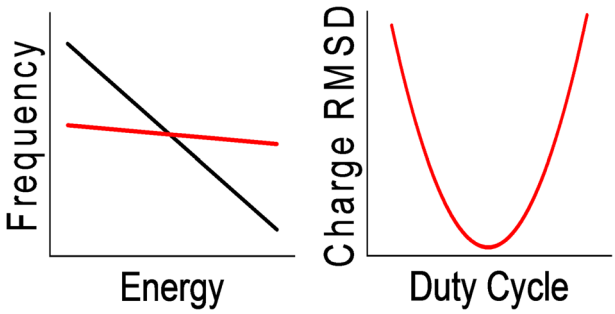

Abstract. In charge detection mass spectrometry (CDMS), ions are passed through a detection tube and the *m*/*z* ratio and charge are determined for each ion. The uncertainty in the charge and *m*/*z* determinations can be dramatically reduced by embedding the detection tube in an electrostatic linear ion trap (ELIT) so that ions oscillate back and forth through the detection tube. The resulting time domain signal can be analyzed by fast Fourier transforms (FFTs). The ion's *m*/*z* is proportional to the square of the oscillation frequency, and its charge is derived from the FFT magnitude. The ion oscillation frequency is dependent on the physical dimensions of the trap as well as the ion energy. A new ELIT has been designed for CDMS using the central particle method. In the new design, the kinetic energy dependence of the ion oscillation frequency is reduced by an order of magnitude. An order of magnitude reduction in energy dependence should have led to an order of magnitude reduction in the uncertainty of the *m*/*z* determination. In practice, a factor of four improvements was achieved. This discrepancy is probably mainly due to the trajectory dependence of the ion oscillation frequency. The new ELIT design uses a duty cycle of 50%. We show that a 50% duty cycle produces the lowest uncertainty in the charge determination. This is due to the absence of even-numbered harmonics in the FFT, which in turn leads to an increase in the magnitude of the peak at the fundamental frequency.

Keywords: Ion trap, Electrostatic linear ion trap, ELIT, Charge detection mass spectrometry, CDMS

Received: 17 January 2018/Revised: 25 May 2018/Accepted: 29 May 2018/Published Online: 9 July 2018

Introduction

Electrospray has extended mass spectrometry to the analysis of native, noncovalent protein complexes and other macromolecular structures [1, 2]. Time-of-flight mass spectrometry (TOFMS) has long been the primary MS technique for the analysis of large ions because in theory there is no upper mass limit. However, the upper mass attainable by TOFMS is limited by the low detection efficiency of commonly used detectors for high *m*/*z* ions [3]. In addition, as analyte mass increases, so does heterogeneity. Many large biological complexes are inherently heterogeneous, and adduct formation becomes more prevalent for larger ions [4]. Heterogeneity leads to broadened *m*/*z* peaks and unresolvable charge states. Without charge state resolution, it is impossible to determine the mass.

Correspondence to: Martin Jarrold; *e-mail:* mfj@iu.edu

The solution to this problem invariably involves a single particle approach where the mass is determined directly for individual ions [5]. The nanomechanical oscillator is one such approach. Here the frequency shift that occurs when a single molecule or ion adsorbs on a nanoscale oscillator is used to deduce its mass [6–8]. Charge shifting is another approach that is closer to traditional mass spectrometry. Here the *m*/*z* is measured for a single ion, the charge is shifted, and the *m*/*z* re-measured [9–14]. This method has been used most widely with a quadrupole ion trap (QIT) and optical detection. While single particle QIT-MS has no upper mass limit and excellent *m*/*z* and charge accuracy, measurements can take a minute or more per ion, and particles smaller than around 50 nm require special techniques. The method is better suited to monitoring single ions for long times rather than recording mass distributions [12, 15–18].

Finally, there are methods based on measuring the *m*/*z* and charge of individual ions. This has been done with Fourier

transform ion cyclotron resonance [19] where the charge is determined from the charge induced on the detector plates. However, because the ion is not surrounded by the detector plates, the induced charge depends on the ion's trajectory and so the charge cannot be determined accurately. A quadrupole ion trap coupled to an external charge detecting plate has also been used to measure the *m*/*z* and charge of single ions [20, 21]. Here again, the charge cannot be determined accurately. TOFMS with cryogenic detectors is another technique in this class [22–27]. However, the detector response is not linearly proportional to the ion charge above a few charges, so charge determination is not currently possible for large ions with hundreds of charges. Last but not least is charge detection mass spectrometry (CDMS). Here the ion is passed through a conducting cylinder and the induced charge is detected by a charge sensitive amplifier. The time of flight through the cylinder is used (along with the ion energy) to deduce the *m*/*z,* and the amplitude of the signal is proportional to the charge. If the cylinder is long enough, the amplitude is independent of the ion's trajectory through the cylinder. Masses into the teradalton regime have been measured [28].

The first use of CDMS was in the 1960s when Shelton and coworkers used single-pass CDMS to determine the masses of fast-moving, micron-sized iron particles [29]. In 1995, Fuerstenau and Benner coupled an electrospray source to a single-pass CDMS detector and used it to measure the mass of DNA ions [30]. The uncertainty in the charge was ± 75 e (elementary charges) which led to a large uncertainty in the derived mass. The large uncertainty in the charge prompted Benner to employ an electrostatic linear ion trap (ELIT), where the ions oscillate back and forth through the detector cylinder, to perform multiple measurements for each ion. The uncertainty in the charge decreases with $n^{1/2}$, where n is the number of measurements [31]. Benner reported a theoretical uncertainty of ± 2.4 e. However, to reduce the number of false positives, the limit of detection (LOD) (the smallest charge that can be reliably detected) was placed at around five times the root mean square deviation (RMSD) of the noise. The high LOD in these measurements (250 e) limited the applicability to very large ions.

More recently, interest in CDMS has been rekindled as there has been an increasing desire to perform mass measurements beyond the range of conventional mass spectrometry [28, 32–43]. Antoine, Dugourd, and coworkers have used single-pass CDMS to characterize nanoparticles, synthetic polymers and amyloid fibrils [33–35]. Williams and coworkers have recently shown that ELIT CDMS can be used to measure collision cross sections [37, 38]. Our group has mainly used CDMS to analyze viruses and virus capsids, including the detection of assembly intermediates for hepatitis B virus capsids [39, 40], the characterization of bacteriophage P22 [41, 42], and the resolution of fully and partially packed adeno-associated virus, a gene therapy vector [43].

Ions in an ELIT oscillate between two axially symmetric electrostatic ion mirrors. This oscillation is analogous to light oscillating between the mirrors in optical resonators such as those used in lasers and interferometers. The first ELIT was described by Zajfman and coworkers as an alternative to heavy-ion storage rings for investigation of high energy ion beams [44]. In addition to CDMS where single ions are trapped, ELITs have been used to perform mass spectrometry with packets of ions [45]. McLuckey and coworkers have expanded the functionality of ELITs with packets of ions, demonstrating both collision-induced dissociation and surface induced dissociation MS/MS [46, 47]. They have also measured collisional cross sections for *m*/*z* selected ion packets by measuring the transient signal decay after the addition of gas to the ELIT [48].

In this manuscript, we describe the factors that need to be considered to optimize the performance of an ELIT for CDMS measurements. A new ELIT design, optimized for CDMS measurements, is described. The performance of the new ELIT is evaluated, and it is shown to have a significantly improved *m*/*z* resolving power over that achieved previously.

ELIT Design Considerations

In CDMS, the uncertainty in the mass determination depends on the uncertainties in the charge and *m*/*z* measurements. Historically, the main issues with CDMS have been the large uncertainty in the charge measurement and the high LOD. The ELIT employed in our prototype CDMS instrument [49] was based on the "conetrap" design of Cederquist and coworkers [50]. However, rather than measure the TOF of the ions through the detector, the time domain signal from the trapped ion is stored and analyzed by fast Fourier transforms (FFTs). The use of FFTs enables the detection of charges which do not rise above the noise in the time domain and lowers the LOD to < 7 e [51]. The *m*/*z* is inversely proportional to the square of the fundamental frequency

$$m/z = \frac{C}{f^2} \tag{1}$$

where C is a constant that is a function of the ion energy as well as the dimensions of the trap. It is determined from ion trajectory simulations. The charge is proportional to the FFT magnitude (when the number of ion cycles is taken into account).

The uncertainty in the charge depends on the trapping time which can be extended by lowering the pressure in the trap [51]. With a trapping time of 3 s, the charge uncertainty was reduced to 0.2 e (RMSD) where it is possible to assign the charge state with almost perfect accuracy [52]. Thus, the uncertainty in *m*/*z* is now the limiting factor in obtaining high precision mass measurements. One of the factors contributing to the uncertainty in the *m*/*z* measurement is the dependence of the oscillation frequency on the ions' kinetic energy. A dual hemispherical deflection analyzer (HDA) is used to limit the energy spread of ions entering the trap. However, the energy dependence of the oscillation frequency with the conetrap design employed on our prototype CDMS instrument is high enough that even a small energy spread leads to a relatively

large uncertainty in the m/z. According to Eq. 1, the m/z depends on the inverse of the oscillation frequency squared; thus, the uncertainty in the m/z is twice the uncertainty in the frequency.

Recent work in the nuclear physics community has led to the development of high (> 100,000) resolving power multi-reflection time-of-flight instruments (MR-TOF) [53–55]. These instruments are essentially ELITs, and although the resolution of these instruments is high, it comes at a cost making them unsuitable for CDMS. The field-free region of MR-TOF analyzers are on the order of 1 m in length. This long flight length would push high m/z ion oscillation to unacceptably low frequencies, decreasing the signal-to-noise ratio due to the 1/f contribution to the noise. In addition, the physical constraints on the ion trajectories imposed by such a long field-free region would reduce the trapping efficiency.

Here we describe a new ELIT designed to optimize performance for CDMS measurements. One of several important design considerations for a CDMS ELIT is that a wide range of kinetic energies and entrance conditions (radial offset and angle) should lead to stable trajectories. If the kinetic energy and entrance conditions are too restrictive, the fraction of ions that are trapped will be low, and it will take an excessive amount of time to collect a spectrum. To minimize the uncertainty in the m/z determination, it is important that changes in the oscillation frequency due to small variations in the ions' kinetic energy are minimized (see above). In addition, the entrance conditions affect the trajectories of the trapped ions, and different trajectories can have slightly different oscillation frequencies. To minimize the uncertainty in the m/z determination, changes in the oscillation frequency due to the ions' trajectories should be minimized. We did not minimize the trajectory dependence in this work though this issue will need to be considered in the future. Finally, the ELIT design can affect the uncertainty in the charge measurement. The duty cycle (the time the ion spends in the detection cylinder divided by the total time to make one oscillation) should be close to 50% (see below).

In what follows, we refer to the previous ELIT design based on the cone trap [50] as the conical trap and the new trap described here as the cylindrical trap. To the best of our knowledge, the cylindrical trap described here provides the highest m/z resolving power and lowest charge uncertainty available for CDMS.

Methods

ELIT Design and Trajectory Simulations

The design parameters for the ion mirrors which comprise the new ELIT were derived from the principles of the central particle method which describes nonaxial trajectories relative to a reference trajectory which is concurrent with the ion optical axis [56]. This method allows the development of explicit, analytical expressions for TOF aberration coefficients. Relative ion mirror parameters (see Figure 1), such as electrode length (l), inner diameter (d), and electrode spacing (δ), with minimized aberration coefficients, are tabulated in [56]. A three-electrode mirror was designed with $l = 4.57$ mm, $d =$ 13.97 mm, and $\delta = 0.127$ mm for each electrode (E1, E2, and E3 in Figure 1). A grounded shield electrode (GS) was added to the mirrors to create the field-free region between the endcaps where the charge detector is located. The grounded electrodes are 3.81 mm thick with a beveled aperture starting at 13.97 mm on the mirror side and reducing at a constant angle to 3.30 mm on the detector side. The field-free region is 50.80 mm in length and holds a cylindrical charge detector 50.04 mm in length and 6.35 mm inner diameter.

Due to the addition of the grounded electrodes, the mirror electrode potentials had to be optimized with ion trajectory simulations. The potentials on E1-E3 were iteratively stepped in 1 V increments to find the combination of electrode potentials that produced the smallest spread in oscillation frequency for 100 axial ions with a Gaussian energy distribution (mean = 130 eV/z, FWHM = 1 eV/z). The optimized potential on E1 is 135 V, and the potential on E2 is switched between 95 and 125 V in transmission and trapping mode, respectively. Likewise, the E3 potential is switched between 0 and 190 V. E1 and the grounded shield form a focusing field while E2 and E3 form the reflecting field in trapping mode. All electrode definition files were written in the SIMION geometry file language in three dimensions with grid units 0.127 mm in length. SIMION 8.1 (Scientific Instrument Services, Inc.) was used to solve the Laplace equation with a 1-μV refinement convergence objective. Potential array files generated by SIMION were then used in a custom program developed to calculate ion trajectories. The custom program uses the Beeman method of integrating the equations of motion which is based on the Verlet algorithm, but produces lower kinetic energy error [57, 58]. Ion trajectories were calculated with a constant time step of 4 ns, and the position of the ions was sampled at a rate of 2.5 MHz (every 400 ns) to match the sampling rate used in the experiments. The ion trajectories were converted to simulated signals using Green's reciprocity theorem to calculate the charge induced on the detector at each sampled ion position [59, 60]. The simulated signals were analyzed using the FFT module from the Intel Math Kernel Library (MKL) for Fortran, and the frequency and magnitude of each peak were found using a derivative-based peak picking algorithm.

Instrument Operation and Sample Preparation

The CDMS instrument used here is similar to the previously described prototype instrument [49] with the key difference being a new electrospray interface optimized to transmit ions over a broad mass range. A detailed description of the interface will be given elsewhere. Briefly, a commercial nano-ESI source (Advion Biosciences) is used for ambient ionization in the positive ion mode. Ions enter the instrument through a heated capillary. After exiting the capillary, they are confined radially and transferred through several stages of differential pumping. In the second differentially pumped region, the ions

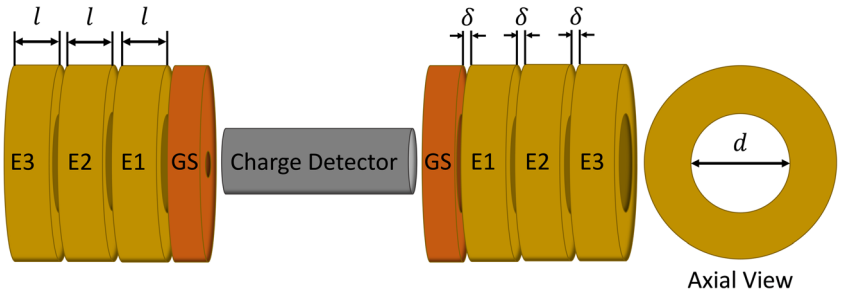

Figure 1. Overview of the cylindrical ELIT design with critical ion mirror electrode parameters labeled

are thermalized in an RF (radio frequency) only hexapole ion guide with a DC potential that sets the ion energy. In the third region, an RF-only segmented quadrupole [61] is held at the same DC potential as the hexapole. Upon exiting the quadrupole, the ions are accelerated through a grounded aperture into an einzel lens that focuses them into a dual hemispherical deflection energy analyzer (HDA). They then pass into the fifth and final differentially pumped region (2×10^{-9} Torr) for analysis by CDMS.

At the beginning of a trapping event, both endcaps are set to transmission mode, and ions travel through the trap. A trapping event is initiated by switching the back endcap from transmission mode to trapping mode. Ions are then reflected back through the detector tube and the entrance of the trap. After a delay of 0.3 ms, the front endcap is switched from transmission to trapping mode. Ions in the trap when the front endcap is switched are trapped and oscillate back and forth through the detector tube. After a user specified time, the trapping event is terminated by returning both endcaps to transmission mode. After a delay of 1 ms, the process is repeated.

Thousands of ions must be measured to generate a mass spectrum (the number needed increases with sample heterogeneity). With the continuous (or random) trapping mode outlined above, the probability that the trap contains zero, one ion, or more than one is given by a Poisson distribution and the maximum number of single ion trapping events that can be realized is 37%. If the average signal is increased from its optimum value, the number of multiple ion trapping events increases at the expense of single ion, and if the signal is decreased, there is an increase in the number of empty trapping events. For 100-ms-long trapping periods, the optimum fraction of single ion trapping events translates to a maximum of around 13,300 single ion events per hour. A spectrum of a homogeneous sample can be collected in under half an hour under optimum conditions (i.e., when the signal is stable and the number of single ion trapping events is close to the maximum that can be realized).

When trapped ions oscillate back and forth through the detection cylinder, they induce a charge that is detected by a charge sensitive amplifier. The resulting time domain signal is amplified and digitized and then analyzed using fast Fourier transforms. As shown in Eq. 1, the m/z of the ion is found from the fundamental frequency, and after accounting for the trapping time, the charge is found from the FFT magnitude. In the experiments reported here, ions were trapped for 100 ms. Much longer trapping times have been achieved and lead to a lower uncertainty in the charge determination. The mean ion energies used were 130 eV/z for the conical trap and 100 eV/z for the conical trap (i.e., the same as in the simulations).

A 1-mg/mL solution of β-galactosidase from *Escherichia coli* was prepared in 150 mM ammonium acetate (both from Millipore Sigma) and desalted by size exclusion chromatography (Bio-Rad Micro BioSpin).

Results and Discussion

The most crucial characteristic of an ELIT for CDMS is its ability to trap ions. A series of trajectory simulation were performed to determine the range of initial ion trajectory conditions that lead to stable ion oscillation. Each ion was initiated at the axial center of the cylindrically symmetric traps and then sequentially stepped in 0.1 mm increments in the radial direction (r). At each value of r, the incident angle was stepped in increments of 0.1°. The trajectory of each ion was calculated for 1 s of flight time. Any ion still trapped at 1 s was judged to be stable and plotted in the stability diagrams for the conical and cylindrical traps shown in Figure 2.

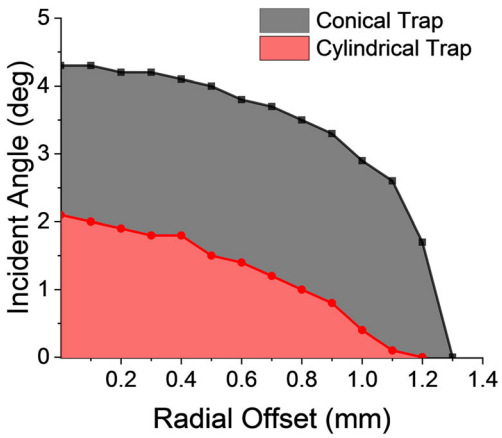

Figure 2. Stability diagrams for the cylindrical and conical traps. A trajectory was considered stable if the ion oscillated for more than 1 s. The radial offset was stepped by increments of 0.1 mm, and the incident angle was stepped by increments of 0.1°. The area under each stability curve was fully sampled to determine if there were any regions of instability. All ions were initiated at $z = 0$ which corresponds to the center of the traps

The radial confinement of large incident angle trajectories in the cylindrical trap was lower than that of the conical trap (Figure 2). At zero radial offset, the conical trap can trap ions with incident angles up to 4.3° while the maximum incident angle in the cylindrical trap at zero radial offset is 2.1°. With an incident angle of 0°, the ions are stable with radial offsets up to 1.3 and 1.2 mm in the conical and cylindrical traps, respectively. These values are close to the radius of the entrance apertures of both traps (1.5 mm).

Despite the lower maximum incident angle that leads to stable ion oscillation in the cylindrical trap, it is still able to trap most ions with realistic trajectories. This is due to the physical constraints the geometry of the traps places on ion trajectories. For example, an ion entering at the largest possible radial offset at the entrance of the cylindrical trap ($r = 1.5$ mm) and focused to the center of the trap 44.9 mm away would have no radial offset at the center of the trap and an incident angle of 1.91° which falls inside the stability zone of the cylindrical trap. Since ions are focused into the cylindrical trap by an einzel lens at the exit of the HDA and refocused by the two inner electrodes of the ion mirror, ions at the center of the trap ($z = 0$) should have small (> 0.5 mm) radial offsets and incident angles below 2°. In the experiment, the ion beam is detected after exiting the trap with a microchannel plate (MCP) detector, and the potential on the einzel lens is adjusted to maximize the signal. The shortest focal length that produces the maximum ion signal has the focus in the center of the trap. Focal distances that fall past the center of the trap also lead to maximized ion signals but lead to smaller incident angles too. Conversely, focal distances which fall short of the center of the trap lead to larger incident angles and trajectories which cannot pass through the trap, which in turn lowers the ion signal. Therefore, maximizing the ion signal on the MCP detector leads to radial offsets and incident angles within the stability range of the trap.

Next, the effect of ion energy spread on the oscillation frequency was evaluated in the conical (Figure 3a) and cylindrical (Figure 3b) traps. The ideal ion energies for the traps (conical 100 eV/z, cylindrical 130 eV/z) were chosen so that ions of the same m/z have approximately the same oscillation frequency, eliminating 1/f noise as a contributing factor to performance differences in the experiment. For this analysis, ions were initiated with no radial offset and an incident angle of 0°. Trajectories were calculated for ions with an m/z of 50 kDa for 1 s, and the trajectories remained on axis throughout the simulation. Signals were generated from the trajectories using Green's reciprocity theorem and analyzed by FFT. The change in frequency was plotted as a function of ion energy deviation from ideal (Figure 3c). The points in the plot are the values from the simulations and the lines are linear least squares fits. In the conical trap, a 1.00% deviation from ideal ion energy leads to a 0.903% change in oscillation frequency. In the cylindrical trap, a 1.00% deviation from ideal ion energy leads to a 0.0899% change in oscillation frequency. Thus, there is an order of magnitude reduction in the energy dependence on going from the conical trap to the cylindrical trap.

A second, larger scale ion trajectory simulation was carried out to characterize and compare the distributions in oscillation frequencies for a single m/z resulting from differences in the entrance conditions. In each trap, trajectories of 3000 ions with an m/z of 50 kDa were simulated for 100 ms. The initial ion positions were assumed to have a radial Gaussian distribution with a diameter of 3 mm (equal to the traps' entrance apertures) at the entrance of the cylindrical trap. The ion positions were then extrapolated to the center of the trap assuming a focal plane in the center with a 1-mm-diameter spot size, and the radial offsets and incident angles were calculated for each ion. This led to an ion distribution with a maximum radial offset of 0.5 mm corresponding to the maximum incident angle of 1.28° at the center of the trap, which falls within the stability boundary for both traps. The initial ion parameters used for the conical trap were identical to those used for the cylindrical trap so that any improvement could only be attributed to lower energy dependence and not to a different distribution of ion trajectories. The initial ion kinetic energies were assumed to have a Gaussian distribution with a standard deviation of 0.4 eV/z centered at 130 eV/z for the cylindrical trap and

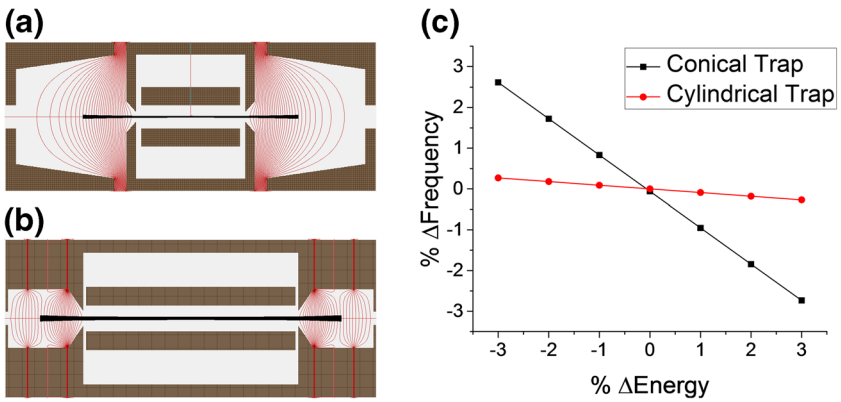

Figure 3. Two dimensional radial slices of the **(a)** conical and **(b)** cylindrical traps. SIMION 8.1 was used to calculate and display the equipotential lines. The ion trajectories shown in the figure were started at z = 0 with no radial offset and an incident angle of 0.57°. **(c)** Comparison of the energy dependences of both traps. The slope = – 0.903 for the conical trap (black, $R^2 = 0.9998$) and the slope = – 0.0899 for the cylindrical trap (red, $R^2 = 0.9997$). The simulations were performed for ions with $m/z = 50$ kDa and $z = 200$

100 eV/z for the conical trap. The 0.4 eV/z deviation in the energy was determined experimentally via retarding potential analysis and is independent of the mean ion beam energy. The calculated ion trajectories were once again converted to simulated signals using Green's reciprocity theorem. FFTs were then performed on the simulated signals using the FFT module from the Intel MKL. The *m*/*z* and *z* of each ion were calculated from the simulated FFT using Eq. 1 and the appropriate calibration constant. The resulting *m*/*z* distributions are plotted in Figure 4a and c. The resolving power of the cylindrical trap (Figure 4a) was found to be 342 while that of the conical trap (Figure 4c) was 65. This represents a 5-fold increase in *m*/*z* resolving power in the cylindrical trap, half of the expected improvement from the on-axis simulations. The smaller than expected improvement is probably due to geometric aberration, the trajectory dependence of the ion frequency. With chromatic aberration reduced, the geometric aberration is a much more important factor in the frequency error.

The uncertainties in the charge determinations for the two traps were also calculated from the simulated trajectories and compared. The sum of the first and second harmonics was used to calculate the charge for ions in the conical trap, while only the first harmonic was used for the cylindrical trap since it lacks even harmonics (as explained below). With zero noise in the simulated signals, one might predict zero uncertainty in the charge measurement. However, the distributions of ion energies and initial conditions lead to variations in the induced waveforms. This causes deviations in the FFT magnitude which in turn leads to uncertainty in the charge determination. The root mean square deviation in the simulated charge for 100 ms trapping is 0.15 e for the cylindrical trap and 0.24 e for the conical trap (Figures 4b, d). This improvement can be attributed to the increased duty cycle of the cylindrical trap (50%) compared to the conical one (30%). The 0.24 e RMSD found here for the conical trap is larger than we have measured experimentally with this trap (0.2 e for 3 s trapping). The experimental measurements include electrical noise, and the simulations (which do not include noise) should not lead to a larger uncertainty than the experimental measurements. The most likely explanation for this anomaly is that the range of energies and entrance conditions present in the experiments is smaller than employed in the simulations.

In both traps, the induced charge signal is approximately a square wave. The cylindrical trap was designed to have a 50% duty cycle while the conical trap has a 30% duty cycle (Figure 5). The importance of the duty cycle was not

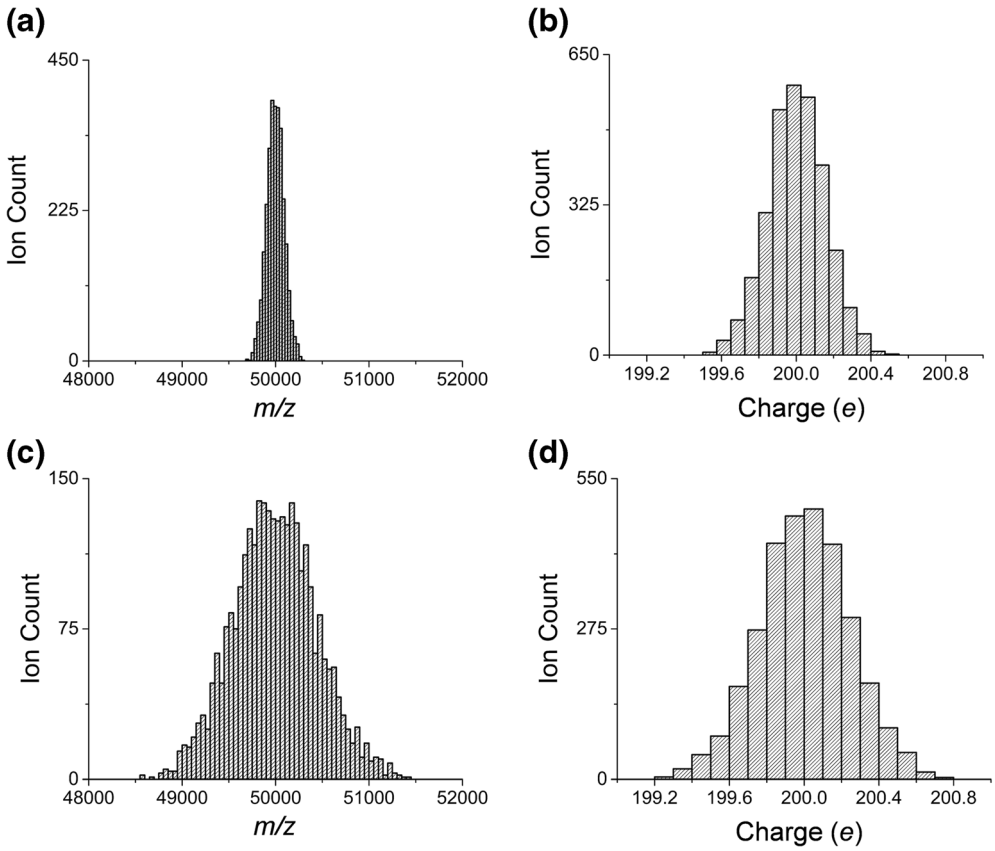

Figure 4. Comparison of the *m*/*z* spectra and charge distributions determined from simulated ion trajectories for the cylindrical trap (upper two plots) and the conical trap (lower two plots). Gaussian energy distributions and reasonable initial trajectory distributions were used for both sets of simulations (see text). Each ion trajectory was simulated for 100 ms, and 3000 trajectories were simulated for each trap. The simulated *m*/*z* resolving powers of the cylindrical trap **(a)** and conical trap **(c)** are 342 and 65, respectively. Thus, the cylindrical trap provides a 5-fold increase in resolving power. The uncertainty in the charge measurement also shows an improvement for the cylindrical trap. The standard deviation is 0.24 e for the conical trap **(d)** and 0.15 e for the cylindrical trap **(b)**

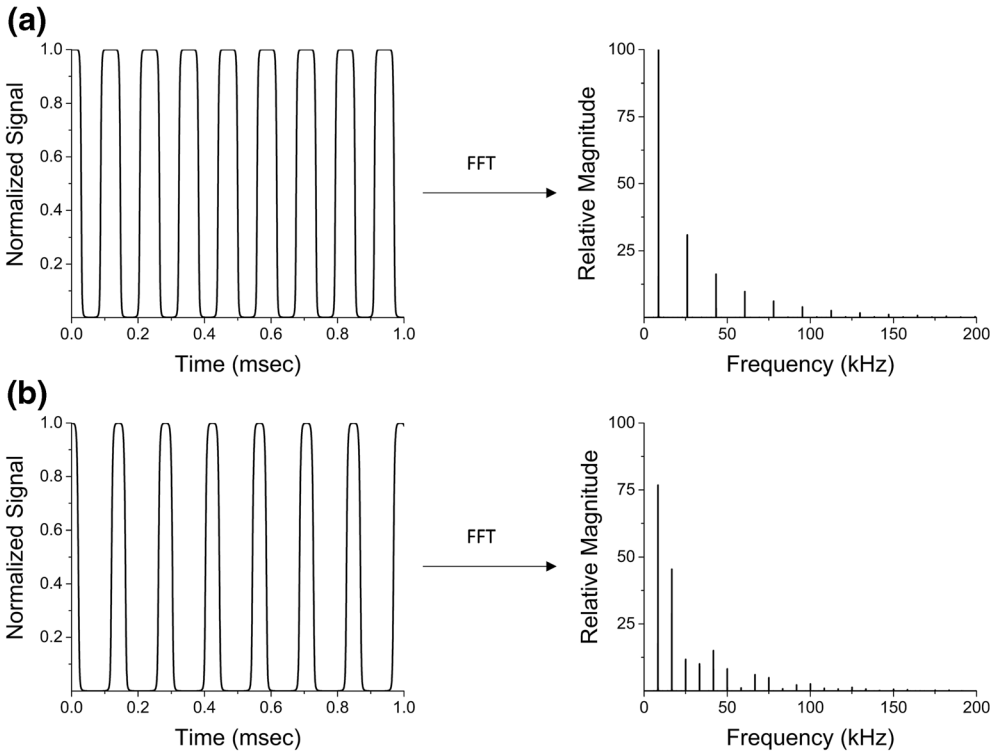

Figure 5. Simulated time domain signals of an ion's oscillations in the cylindrical **(a)** and conical **(b)** traps. Signals are normalized such that the maximum signal is 1, and the minimum signal is 0. An FFT of each signal is also shown. The FFT magnitudes are relative to the magnitude of fundamental peak in the cylindrical trap. The 50% duty cycle in the cylindrical trap eliminates the even harmonics in the frequency domain which in turn increases the magnitude of the fundamental peak

recognized when the conical trap was designed. An ideal, 50% duty cycle square wave does not have even-numbered harmonics in its FFT, and fewer harmonics leads to a fundamental peak with a larger magnitude. Since the charge of the ion is proportional to the magnitude of the fundamental peak, the increase in the magnitude has the potential to decrease the charge uncertainty by increasing the signal-to-noise ratio of the fundamental peak. To investigate this, a function generator was used to induce signals of different duty cycles on the charge detection cylinder. A signal frequency of 10 kHz was employed with a signal amplitude equivalent to a charge of 220 e. One thousand 100 ms signal files were collected and analyzed at each duty cycle. The data was analyzed using the same procedure as real ions, and the uncertainty in the charge was calculated and plotted against the duty cycle in Figure 6. The points are the measured values, and the line is a least squares fit to a parabola. The lowest uncertainty was attained with duty cycle of around 50%. We attribute this to the higher S/N produced by the larger magnitude fundamental peak.

In the case of paraxial ion trajectories, the 50% duty cycle also reduces the energy dependence of the ion oscillation frequency because the field in the ion mirror is approximately linear along the ion optical axis. The time the ion spends in free flight is inversely proportional to the square root of the total ion energy, and the time spent in the ion mirror is directly proportional to the square root of the total ion energy. A small change in ion energy from the ideal value is compensated for by equal and opposite changes in the time of free flight and the time spent in the ion mirror. The same principal is applied in designing reflectron TOF instruments [62].

Finally, the cylindrical trap was built and tested experimentally using β-galactosidase (β-gal). β-Gal exists natively as a homo-tetramer with a mass of 465 kDa. The *m/z* spectrum of β-gal measured with the cylindrical trap and a representative spectrum measured with the conical trap are shown in Figure 7.

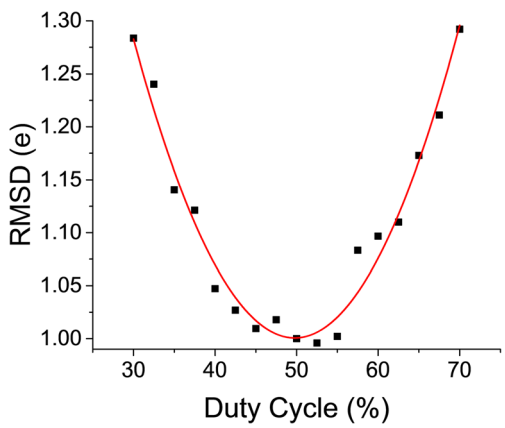

Figure 6. Charge uncertainty as a function of duty cycle. A function generator was used to induce signals of different duty cycles on the charge detection cylinder. The signal had a frequency of 10 kHz and an amplitude equivalent to 220 e. One thousand 100-ms signal files were collected and analyzed at each duty cycle. The lowest uncertainty was achieved at a 50% duty cycle

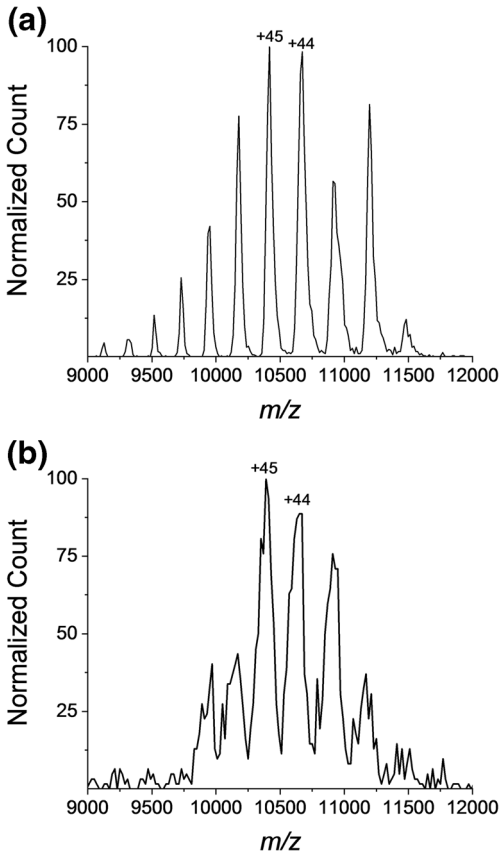

Figure 7. Comparison of *m/z* spectra of β-galactosidase measured with the cylindrical trap **(a)** and with the conical trap **(b)**. Both histograms were made with a 5-Da bin width. β-Galactosidase ions (6142 and 5819) were trapped in the cylindrical and conical traps, respectively. The maximum resolving power for the cylindrical trap is 330 and for the conical trap it is 78

The spectra contain approximately the same number of ions: 6142 β-galactosidase ions were analyzed for the cylindrical trap spectrum and 5819 ions were analyzed for the conical trap spectrum. The cylindrical trap shows improved *m/z* resolution compared to the conical trap. The FWHM resolution of the +45 peak in the conical trap spectrum is 78 while the resolution of the same peak in the cylindrical trap spectrum is 330. This represents a 4.2-fold increase in resolution which is in good agreement with 5-fold improvement predicted by simulation. Note that the *m/z* resolving power should be independent of *m/z*. Both spectra in Figure 7 contain approximately the same number of ions (around 6000), and the increased fluctuations in the lower resolution spectra result because the ions are distributed over more bins. The relative random fluctuations in the intensities (which scale as $n^{-1/2}$, where n is the number of ions in each bin) are larger when the number of ions per bin is smaller.

Conclusion

Historically, the mass resolving power of CDMS has been limited by the uncertainty in the charge measurement. Recent work in our group has decreased the uncertainty in the charge to 0.2 e RMSD [52], at which point the charge state of the ion can be assigned with almost perfect accuracy. Thus, attention has shifted to reducing the uncertainty in the *m/z* determination, in order to improve the mass resolving power attainable with CDMS. To improve the *m/z* resolving power, we designed a new ELIT, optimized for both *m/z* and charge measurements.

The design of the new ion trap meets three key criteria. First, because the signals available for large ions are often small, the trap was designed to trap all realistic incoming ion trajectories so that the time required to collect a spectrum is minimized. Second, the energy dependence of the ion oscillation frequency was reduced by an order of magnitude over our previous trap design. Third, the duty cycle of the ion signal was increased to 50% to decrease the uncertainty in the charge determination by increasing the magnitude of the FFT fundamental frequency. When implemented, the new trap provided more than a 4-fold improvement in the *m/z* resolution over our previous design. To our knowledge, the new cylindrical trap has the highest *m/z* resolving power and lowest uncertainty in the charge determination available for CDMS measurements.

Funding Information

This material is based upon work supported by the National Science Foundation under Grant Number CHE–1531823.

References

1. Loo, J.A.: Studying noncovalent protein complexes by electrospray ionization mass spectrometry. Mass Spectrom Rev. **16**, 1–23 (1997)
2. Zhou, M., Robinson, C.V.: When proteomics meets structural biology. Trends Biochem. Sci. **35**, 522–529 (2010)
3. Fraser, G.W.: The ion detection efficiency of microchannel plates (MCPs). Int. J. Mass Spectrom. **215**, 13–30 (2002)
4. Lössl, P., Snijder, J., Heck, A.J.R.: Boundaries of mass resolution in native mass spectrometry. J. Am. Soc. Mass Spectrom. **25**, 906–914 (2014)
5. Keifer, D.Z., Jarrold, M.F.: Single-molecule mass spectrometry. Mass Spectrom Rev. **36**, 715–733 (2017)
6. Dohn, S., Svendsen, W., Boisen, A.: Mass and position determination of attached particles on cantilever based mass sensors. Rev. Sci. Instrum. **103303**, 78 (2007)
7. Hanay, M.S., Kelber, S., Naik, A.K., Chi, D., Hentz, S., Bullard, E.C., Colinet, E., Duraffourg, L., Roukes, M.L.: Single-protein nanomechanical mass spectrometry in real time. Nat Nanotechnol. **7**, 602–608 (2012)
8. Sage, E., Brenac, A., Alava, T., Morel, R., Dupré, C., Hanay, M.S., Roukes, M.L., Duraffourg, L., Masselon, C., Hentz, S.: Neutral particle mass spectrometry with nanomechanical systems. Nat Commun. **6**, 6482 (2015)
9. Bruce, J.E., Cheng, X., Bakhtiar, R., Wu, Q., Hofstadler, S.A., Anderson, G.A., Smith, R.D.: Trapping, detection, and mass measurement of individual ions in a Fourier transform ion cyclotron resonance mass spectrometer. J. Am. Chem. Soc. **116**, 7839–7847 (1994)
10. Philip, M.A., Gelbard, F., Arnold, S.: An absolute method for aerosol particle mass and charge measurement. J. Colloid Interface Sci. **91**, 507–515 (1983)
11. Hars, G., Tass, Z.: Application of quadrupole ion trap for the accurate mass determination of submicron size charged particles. J. Appl. Phys. **77**, 4245–4250 (1995)
12. Schlemmer, S., Illemann, J., Wellert, S., Gerlich, D.: Nondestructive high-resolution and absolute mass determination of single charged particles in a three-dimensional quadrupole trap. J. Appl. Phys. **90**, 5410–5418 (2001)

13. Peng, W.-P., Chou, S.-W., Patil, A.A.: Laser induced acoustic desorption mass spectrometry of single bioparticles. Angew. Chemie Int. Edit. **45**, 1423–1426 (2006)
14. Nie, Z., Tzeng, F.Y.-K., Chang, H.-C., Chiu, C.-C., Chang, C.-Y., Chang, C.-M., Tao, M.-H.: Microscopy-based mass measurement of a single whole virus in a cylindrical ion trap. Angew. Chem. Int. Edit. **45**, 8131–8813 (2006)
15. Schlemmer, S., Wellert, S., Windisch, F., Grimm, M., Barth, S., Gerlich, D.: Interaction of electrons and molecules with a single trapped nanoparticle. Appl. Phys A. **78**, 629–636 (2004)
16. Howder, C.R., Bell, D.M., Anderson, S.L.: Optically detected, single nanoparticle mass spectrometer with pre-filtered electrospray nanoparticle source. Rev. Sci. Instrum. **85**, 014104 (2014)
17. Bell, D.M., Howder, C.R., Johnson, R.C., Anderson, S.L.: Single CdSe/ZnS nanocrystals in an ion trap: charge and mass determination and photophysics evolution with changing mass, charge, and temperature. ACS Nano. **8**, 2387–2398 (2014)
18. Howder, C.R., Long, B.A., Bell, D.M., Furakawa, K.H., Johnson, R.C., Fang, Z., Anderson, S.L.: Photoluminescence of charged CdSe/ZnS quantum dots in the gas phase: effects of charge and heating on absorption and emission probabilities. ACS Nano. **8**, 12534–12548 (2014)
19. Chen, R., Wu, Q., Mitchell, D.W., Hofstadler, S.A., Rockwood, A.L., Smith, R.D.: Direct charge number and molecular weight determination of large individual ions by electrospray ionization Fourier transform ion cyclotron resonance mass spectrometry. Anal Chem. **66**, 3964–3969 (1994)
20. Peng, W.-P., Lin, H.-C., Lin, H.-H., Chu, M., Yu, A.L., Chang, H.-C., Chen, H.-C.: Charge-monitoring laser-induced acoustic desorption mass spectrometry for cell and microparticle mass distribution measurement. Angew. Chem. Int. Ed. **46**, 3865–3869 (2007)
21. Nie, Z., Cui, F., Chu, M., Chen, C.-H., Chang, H.-C., Cai, Y: Calibration of a frequency-scan quadrupole ion trap mass spectrometer for microparticle mass analysis. Int. J. Mass Spectrom. **270**, 8–15 (2008)
22. Frank, M., Labov, S.E., Westmacott, G., Benner, W.H.: Energy-sensitive cryogenic detectors for high-mass biomolecule mass spectrometry. Mass Spectrom Rev. **18**, 155–186 (1999)
23. Rabin, M.W., Hilton, G.C., Martinis, J.M.: Application of microcalorimeter energy measurement to biopolymer mass spectrometry. IEEE Trans. Appl. Supercond. **11**, 242–224 (2001)
24. Twerenbold, D., Vuilleumier, J.L., Gerber, D., Tadsen, A.: Detection of single macromolecules using a cryogenic particle detector coupled to a biopolymer mass spectrometer. App. Phys. Lett. **68**, 3503–3505 (1996)
25. Frank, M., Mears, C.A., Labov, S.E., Benner, W.H., Horn, D., Jaklevich, J.M., Barfknecht, A.T.: High efficiency detection of 66,000 Da protein molecules using a cryogenic detector in a matrix-assisted laser desorption/ionization time-of-flight mass spectrometer. Rapid Commun. Mass Sp. **10**, 1946–1950 (1996)
26. Wenzel, R.J., Matter, U., Schultheis, L., Zenobi, R.: Analysis of megadalton ions using cryodetection MALDI time-of-flight mass spectrometry. Anal. Chem. **77**, 4329–4337 (2005)
27. Aksenov, A., Bier, M.: The analysis of polystyrene and polystyrene aggregates into the mega dalton mass range by cryodetection MALDI TOF MS. J. Am. Soc. Mass Spectrom. **19**, 219–230 (2008)
28. Mabbett, S.R., Zilch, L.W., Maze, J.T., Smith, J.W., Jarrold, M.F.: Pulsed acceleration charge detection mass spectrometry: application to weighing electrosprayed droplets. Anal Chem. **79**, 8431–8439 (2007)
29. Shelton, H., Hendricks, C.D., Wuerker, R.F.: Electrostatic acceleration of microparticles to hypervelocities. J. Appl. Phys. **31**, 1243–1246 (1960)
30. Fuerstenau, S.D., Benner, W.H.: Molecular weight determination of megadalton-DNA electrospray ions using charge detection mass spectrometry. Rapid Commun. Mass Sp. **9**, 1528–1538 (1995)
31. Benner, W.H.: A gated electrostatic ion trap to repetitiously measure the charge and *m/z* of large electrospray ions. Anal. Chem. **69**, 4162–4168 (1997)
32. Maze, J.T., Jones, T.C., Jarrold, M.F.: Negative droplets from positive electrospray. J. Phys. Chem. A. **110**, 12607–12612 (2006)
33. Doussineau, T., Kerleroux, M., Dagany, X., Clavier, C., Barbaire, M., Maurelli, J., Antoine, R., Dugourd, P.: Charging megadalton poly(ethylene oxide)s by electrospray ionization. A charge detection mass spectrometry study. Rapid Commun Mass Sp. **25**, 617–623 (2011)
34. Doussineau, T., Désert, A., Lambert, O., Taveau, J.-C., Lansalot, M., Dugourd, P., Bourgeat-Lami, E., Ravaine, S., Duguet, E., Antoine, R.: Charge detection mass spectrometry for the characterization of mass and surface area of composite nanoparticles. J. Phys. Chem. C. **119**, 10844–10849 (2015)
35. Doussineau, T., Mathevon, C., Altamura, L., Vendrely, C., Dugourd, P., Forge, V., Antoine, R.: Mass determination of entire amyloid fibrils by using mass spectrometry. Angew. Chem. Int. Edit. **55**, 2340–2344 (2016)
36. Elliot, A.G., Harper, C.C., Lin, H.-W., Williams, E.R.: Mass, mobility and MSn measurements of single ions using charge detection mass spectrometry. Analyst. **142**, 2760–2769 (2017)
37. Elliott, A.G., Harper, C.C., Lin, H.-W., Susa, A.C., Xia, Z., Williams, E.R.: Simultaneous measurements of mass and collisional cross-section of single ions with charge detection mass spectrometry. Anal Chem. **89**, 7701–7708 (2017)
38. Barney, B.L., Terik Daly, R., Austin, D.E.: A multi-stage image charge detector made from printed circuit boards. Rev. Sci. Instrum. **114101**, 84 (2013)
39. Pierson, E.E., Keifer, D.Z., Selzer, L., Lee, L.S., Contino, N.C., Wang, J.C.-Y., Zlotnick, A., Jarrold, M.F.: Detection of late intermediates in virus capsid assembly by charge detection mass spectrometry. J. Am. Chem. Soc. **136**, 3536–3541 (2014)
40. Lutomski, C.A., Lyktey, N.A., Zhao, Z., Pierson, E.E., Zlotnick, A., Jarrold, M.F.: HBV capsid completion occurs through error correction. J. Am. Chem. Soc. **139**, 16932–16938 (2017)
41. Keifer, D.Z., Motwani, T., Teschke, C.M., Jarrold, M.F.: Measurement of the accurate mass of a 50 MDa infectious virus. Rapid Commun Mass Sp. **30**, 1957–1962 (2016)
42. Motwani, T., Lokareddy, R.K., Dunbar, C.A., Cortines, J.R., Jarrold, M.F., Cingolani, G., Teschke, C.M.: A viral scaffolding protein triggers portal ring oligomerization and incorporation during procapsid assembly. Sci Adv. **3**, e1700423 (2017)
43. Pierson, E.E., Keifer, D.Z., Asokan, A., Jarrold, M.F.: Resolving Adeno-associated viral particle diversity with charge detection mass spectrometry. Anal Chem. **88**, 6718–6725 (2016)
44. Dahan, M., Fisherman, R., Heber, O., Altstein, N., Zajfman, D., van der Zande, W.J.: A new type of electrostatic ion trap for storage of fast ion beams. Rev. Sci. Instrum. **69**, 76–83 (1998)
45. Ring, S., Pederson, H.B., Heber, O., Rappaport, M.L., Witte, P.D., Bhushan, K.G., Altstein, N., Sagi, I., Zajfman, D.: Fourier transform time-of-flight mass spectrometry in an electrostatic ion beam trap. Anal Chem. **72**, 4041–4046 (2000)
46. Hilger, R.T., Santini, R.E., Mcluckey, S.A.: Nondestructive tandem mass spectrometry using a linear Quadrupole ion trap coupled to a linear electrostatic ion trap. Anal Chem. **85**, 5226–5232 (2013)
47. Hilger, R.T., Santini, R.E., McLuckey, S.A.: Tandem mass spectrometry in an electrostatic linear ion trap modified for surface-induced dissociation. Anal Chem. **86**, 8822–8828 (2014)
48. Dziekonski, E.T., Johnson, J.T., Lee, K.W., McLuckey, S.A.: Determination of collision cross sections using a Fourier transform electrostatic linear ion trap mass spectrometer. J. Am. Soc. Mass Spectrom. https://doi.org/10.1007/s13361-017-1720-1
49. Contino, N.C., Jarrold, M.F.: Charge detection mass spectrometry for single ions with a limit of detection of 30 charges. Int. J. Mass Spectrom. **345–347**, 153–159 (2013)
50. Schmidt, H.T., Cederquist, H., Jensen, J., Fardi, A.: Conetrap: a compact electrostatic ion trap. Nuc. Instrum. Meth. Phys. Res. B. **173**, 523–527 (2001)
51. Pierson, E.E., Contino, N.C., Keifer, D.Z., Jarrold, M.F.: Charge detection mass spectrometry for single ions with an uncertainty in the charge measurement of 0.65 e. J. Am. Soc. Mass Spectrom. **26**, 1213–1220 (2015)
52. Keifer, D.Z., Shinholt, D.L., Jarrold, M.F.: Charge detection mass spectrometry with almost perfect charge accuracy. Anal Chem. **87**, 10330–10337 (2015)
53. Yakor, M., Plaß, W., Dickel, T., Gessel, H., Scheidenberger, C.: Ion-optical design of a high performance multiple-reflection time-of-flight mass spectrometer and isobar separator. Int. J. Mass Spectrom. **381-382**, 1–9 (2015)
54. Weinholtz, F., Atanasov, D., Kreim, S., Manea, V., Rosenbusch, M., Schweikhard, L., Welker, A., Wolf, R.N.: Towards ultrahigh-resolution multi-reflectron time-of-flight mass spectrometry at ISOLTRAP. Phys Scripta. **2015**, 014068 (2015)
55. Tiana, Y.L., Wanga, Y.S., Wanga, J.Y., Zhoua, X.H., Huang, W.X.: Designing a multi-reflection time-of-flight mass analyzer for LPT. Int J. Mass Spectrom. **408**, 28–32 (2016)

56. Yakushev, E. M.: Theory and computation of electron mirrors: the central particle method. in Advances in Imaging and Electron Physics (Hawkes, P., Ed.) Vol. 178, Pp 147–247 (Elsevier, 2013)
57. Verlet, L.: Computer "experiments" on classical fluids. I. Thermodynamical properties of Lennard-Jones molecules. Phys Rev. **159**, 98–103 (1967)
58. Schofield, P.: Computer simulation studies of the liquid state. Comput. Phys Commun. **5**, 17–23 (1973)
59. Shockley, W.: Currents to conductors induced by a moving point charge. J. Appl. Phys. **9**, 635 (1938)
60. Alexander, J.D., Graham, L., Calvert, C.R., Kelly, O., King, R.B., Williams, I.D., Greenwood, J.B.: Determination of absolute ion yields from a MALDI source through calibration of an image charge detector. Meas. Sci Technol. **045802**, 21 (2010)
61. Berkout, V.D., Doroshenko, V.M.: Improving the quality of the ion beam exiting a quadrupole. J. Am. Soc. Mass Spectrom. **17**, 335–340 (2006)
62. De Hoffman, E., Stroobant, V.: Mass spectrometry principles and applications, 3rd edn. Wiley, West Sussex (2008)